Solidification Crack Susceptibility in Weld Metals of Duplex Stainless Steels†

– Effects of Ferrite Content and Microsegregation on Solidification Crack Susceptibility –

Fukuhisa MATSUDA*, Hiroji NAKAGAWA**, Ichiro KATO***, Yoshiaki MURATA***

Abstract

Solidification crack susceptibilities in weld metals of JIS SUS 329J_2L where ferrite content was varied in the range of about 0 to 100% were evaluated by the Trans-Varestraint cracking test and another practical hot cracking test, and then metallurgical characteristics in weld metals such as microsegregation of detrimental impurities and solidification behavior etc. were studied in relation to the susceptibility. Main conclusions obtained are as follows:

(1) Solidification crack susceptibility showed a minimum at a ferrite level of 5 to 20%, and increased as ferrite content decreased or increased.

(2) The cause of this tendency was inferred mainly that both quantitative and qualitative properties of such microsegregation as P, S and O in weld metals were changed according to ferrite content. That is to say, in the case of extremely low ferrite content, FeS type sulphide and partial Cr_3P type phosphide were abundant at cellular dendritic boundary. On the other hand, in the case of extremely high ferrite content, Cr_2O_3-Fe_2O_3 type complex oxide containing a high amount of S was abundant at cellular dendritic boundary. On the contrary, these inclusions were not detected in case of 5 to 80% ferrite content.

(3) Moreover, it was shown by hot stage microscope that the liquation temperature of grain-boundary in weld metal as a measure of true solidus corresponded well with the lower temperature limit of the BTR, and thus this confirms that the impurity segregation in the extremely high ferrite content was relatively high.

(4) Besides, grain size in welding direction during solidification in cases of extremely low and high ferrite content were greater than that in case of 20 to 70% ferrite content. It was suggested that also this tendency was another reason explaining the crack susceptibility.

KEY WORDS: (Hot Cracking) (Solidification) (Segregation) (Microstructure) (Ferrite) (Stainless Steels)

1. Introduction

Duplex austenitic-ferritic stainless steels which contains approximately similar amounts of austenite and ferrite to each other have been developed in an attempt to combine the advantages of both the austenitic and ferritic phases, in which the austenite imparts toughness and general corrosion resistance and the ferrite imparts strength and resistance to stress corrosion cracking.[1] Therefore, duplex austenitic ferritic stainless steels have been widely used as materials for chemical plants in chloride environments and equipments of sour well because of their excellent stress corrosion cracking resistance and high strength than those of austenitic stainless steels, and of superior ductility to ferritic stainless steels.

In fusion welding of duplex stainless steels, it is known that solidification cracking occurs frequently in the weld metals when excessive distortion and shrinkage take place in the weld metals due to a rapid local weld cycle. Concerning this, a great deal of research has been done on the effect of ferrite in weld metal on solidification crack susceptibility, but most materials studied contained 20% ferrite content at utmost, except for Kujanpää et al.[2–4]

In this report, solidification crack susceptibility of stainless steels, which contain ferrite in the range of about 0 to 100%, has been investigated mainly by the Trans-Varestraint cracking test. Partly, another practical hot cracking test in the form of the modified Navy-Torture cracking test was also done for materials of typical ferrite contents to confirm the tendency of solidification crack susceptibility.

On the other hand, it is usually considered[5] as a major metallurgical cause of solidification cracking in stainless steels that such impurities as P and S remarkably extend the solidification temperature range to form phosphide and sulphide of low melting point, respectively. For this reason, the microsegregation degrees of P and S in weld metals were evaluated by amounts of inclusions enriched with P and S, their shapes, main constituting elements, distribution profiles and structure types in relation with

† Received on May 7, 1986
* Professor
** Research Instructor
*** Sumikin Welding Industries, Ltd.

Transactions of JWRI is published by Welding Research Institute of Osaka University, Ibaraki, Osaka 567, Japan

the solidification crack susceptibility. Moreover, for some materials, the melting temperature of grain-boundary in weld metal was directly measured by hot-stage microscope in order to obtain a more detailed understanding of the true solidus temperature during welding.

Furthermore, it is well known[6–9] that microfractography is very effective to analyze the phenomena and the mechanism of solidification cracking. Therefore, in this report detailed fractographic analyses with SEM were conducted.

2. Materials Used and Experimental Procedure

2.1 Materials used

Materials used were 17 kinds of experimental stainless steel deposited metals of modified duplex austenitic-ferritic stainless steel JIS SUS 329J_2L* containing 23 ~ 27%Cr–2~21%Ni–3%Mo–0.1%N with commercial levels of other elements. The selection of chemical composition was done on the basis to provide mainly various ferrite content and additionally different Cr_{eq} values by controlling the amounts of Ni and Cr. Moreover, 6 different commercial stainless steel base metals (thickness: 12 mm) were used to obtain the reference data. The chemical compositions and ferrite contents in vol.% are shown in **Tables 1** and **2.** Ferrite content was measured by the point-counting method according to ASTM E562 standard and partly by the Ferrite Scope at the top surface of GTA welded bead after the Trans-Varestraint cracking test. The positions of materials in Schaeffler diagram are illustrated in **Fig. 1.** In this figure, the numerals in the parentheses by the side of the marks show the ferrite contents measured. The measured ferrite contents correspond well with those predicted from the Schaeffler diagram.

Table 1 Chemical compositions of deposited metals of modified SUS 329J_2L type stainless steel cored wire.

Mark	Chemical composition(%) C	Si	Mn	P	S	Ni	Cr	Mo	N	Others	Equivalents Nieq*1	Creq*2	Ferrite Content(%) Point count method	Ferrite scope
29CFA	0.032	0.60	1.28	0.020	0.008	21.33	24.77	2.92	0.12	0:0.032	25.2	28.6	1	0
29C10F	0.030	0.60	1.25	0.021	0.008	15.08	24.30	2.58	0.10	0:0.048	18.3	27.8	6	12
29C20F	0.032	0.60	1.24	0.020	0.008	12.25	24.70	2.90	0.11		15.8	28.5	13	24
29C30F	0.031	0.61	1.23	0.021	0.008	10.70	24.69	2.71	0.10		13.9	28.3	21	30
29C40F	0.033	0.60	1.24	0.021	0.007	9.56	24.76	2.73	0.10	0:0.055	12.8	28.4	44	44
29C50F	0.031	0.61	1.26	0.022	0.007	8.94	24.69	2.76	0.10		12.2	28.4	53	50
29C60F	0.032	0.61	1.25	0.021	0.008	8.10	24.84	2.78	0.11		11.6	28.5	64	56
29C70F	0.035	0.61	1.22	0.023	0.006	7.22	24.36	2.66	0.10	Ti:0.03	10.5	28.0	77	72
29C80F	0.036	0.61	1.22	0.023	0.006	6.28	24.75	2.68	0.11	"	9.9	28.4	90	76
29C90F	0.035	0.61	1.22	0.023	0.005	4.30	24.75	2.73	0.10	"	7.6	28.4	97	78
29CFF	0.037	0.61	1.21	0.023	0.006	2.33	24.60	2.76	0.10	0:0.067	5.7	28.3	99	83
27C30F	0.027	0.59	1.23	0.022	0.007	9.39	22.71	2.49	0.10		12.5	26.1	20	29
27C50F	0.030	0.60	1.26	0.022	0.008	7.85	22.76	2.76	0.09		10.7	26.4	50	51
27C70F	0.034	0.60	1.19	0.023	0.006	6.23	22.69	2.55	0.11		9.8	26.1	71	62
31C30F	0.038	0.59	1.23	0.022	0.007	11.77	26.46	2.69	0.10		15.2	30.0	28	31
31C50F	0.034	0.60	1.25	0.022	0.008	10.03	26.17	2.59	0.10		13.3	30.0	52	50
31C70F	0.030	0.59	1.24	0.022	0.007	8.36	26.38	2.66	0.10		11.5	29.9	68	67

Table 2 Chemical compositions of base metals of commercial stainless steels and their ferrite contents after welding.

Mark	Chemical composition(%) C	Si	Mn	P	S	Ni	Cr	Mo	N	Others	Equivalents Nieq	Creq	Ferrite content(%) Point count method	Ferrite scope
SUS310S	0.07	0.61	1.67	0.022	0.001	19.14	24.78	0.06	0.03	0:0.006	21.6	25.8	ND	0
SUS309S	0.07	0.74	1.52	0.020	0.007	13.50	23.27	0.05	0.03		10.5	19.3	-	3
SUS316L	0.016	0.71	0.94	0.031	0.005	12.18	17.42	2.21	0.03		12.7	20.7	-	5
SUS304L	0.017	0.51	1.48	0.025	0.005	9.73	18.50	0.05	0.03		15.9	24.4	-	5
SUS329J2L	0.017	0.57	1.57	0.028	0.001	5.49	22.13	2.92	0.14	Cu:0.07	9.7	25.9	86	77
SUS430	0.07	0.64	0.57	0.027	0.005	0.42	16.24	0.05	0.01		1.8	17.3	85	78

*1 Nieq=%Ni+30x%C+0.5x%Mn+30x(%N-0.06)

*2 Creq=%Cr+%Mo+1.5x%Si+0.5x%Nb

* SUS 329J_2L is the designation for duplex austenitic-ferritic stainless steel in Japan Industrial Standard (JIS). The chemical composition required is as follows: C; 0.03%max, Si; 1.0%max, Mn; 1.5%max P; 0.04%max, S; 0.03%max, Ni; 4.5~7.5%, Cr; 22.0 ~ 26.0%, Mo; 2.5 ~ 4.0%, N; 0.08 ~ 0.30%.

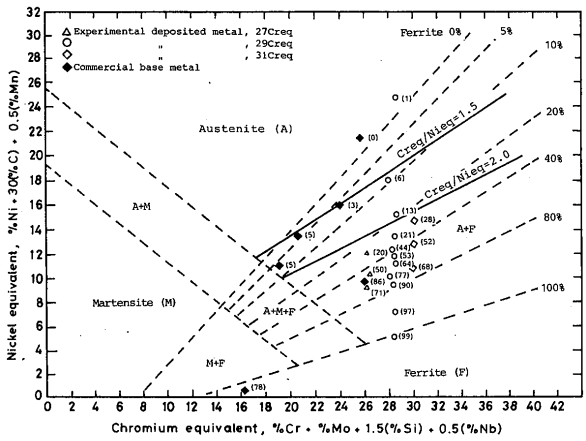

Fig. 1 Schaeffler diagram in which materials used are plotted.

2.2 Hot cracking test

2.2.1 The Trans-Varestraint cracking test[10)]

The specimens were prepared in the following manner: As shown in **Fig. 2**, a groove was machined in the base metal of SUS 304L plate, and filled up with 4 layers of GTA welding utilizing experimental metal cored wire producing the deposited metal in Table 1. The GTA welding conditions were welding current of 180A, arc voltage of 17 V and welding speed of 20 mm/min. Then the plate was machined to a thickness of 12 mm as shown in **Fig. 3** for the Trans-Varestraint cracking test. GTA welding was made under the welding conditions shown in **Table 3**.

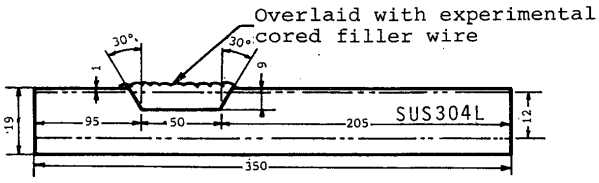

Fig. 2 Preparation of the deposited metal for the Trans-Varestraint test.

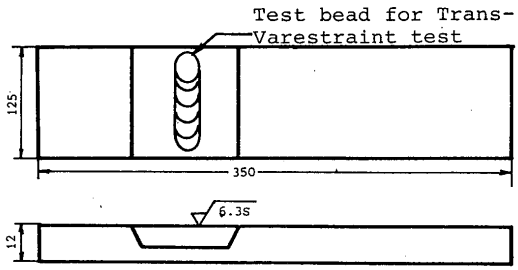

Fig. 3 The shape and dimensions of the specimen used for the Trans-Varestraint test.

Also the commercial stainless steel base metals were used for the Trans-Varestraint cracking test. The length of cracks on the surface of welded bead in as-welded conditions was carefully measured at X 40 magnification by using binocular microscope. Solidification crack susceptibility was evaluated by the maximum crack length, the total crack length and the BTR (solidification brittleness temperature range), which was obtained by combining the maximum crack length with the cooling curve measured along the center of the welded bead with W/5%Re-W/26%Re thermocouple of 0.3 mm dia. Liquidus (T_L) and nominal solidus (T_S) were measured by thermal analysis in furnace.

Table 3 Conditions used in the Trans-Varestraint test.

Welding parameters:	GTA weld DCEN,250A,19V Welding speed 150mm/min. Arc length 3mm
Electrode:	EWTh-2,4mm dia.
Shielding gas:	pure Ar (20litre/min.)
Bending radius:	300mm
Air cylinder pressure:	6kgf/cm^2
Augmented strain on specimen	: 2.0%

2.2.2 The modified Navy-Torture cracking test

The modified Navy-Torture cracking test, which is one of self-restraint cracking test, was used in order to study the susceptibility of practical production welds. The Navy-Torture cracking test was modified in this study to ensure the occurrence of solidification cracking as follows:

1) The restraint plate (thickness: 36 mm) beneath the weld line was machined to make the groove of 20 mm width shown in **Fig. 4**, so that the heat transfer to the restraint plate during test welding might be diminished as little as possible.
2) Two specimens were butted together with a gap of 3 mm to make Y-groove on the center line of the restraint plate, and restraint fillet SMA welding was done around the specimens except for the groove.

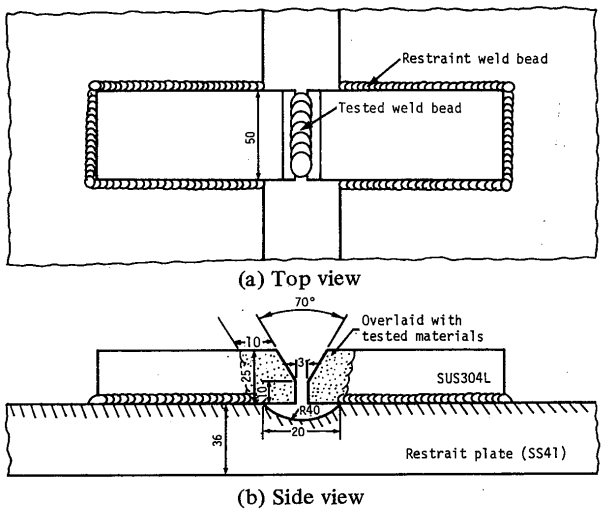

Fig. 4 The shape and dimensions of the specimen used for the modified Navy-Torture cracking test and its setting method.

3) The surfaces of Y-groove were overlaid with the same cored filler wire as that in the test welding to eliminate the effect of base metal SUS 304L.

GTA test welding was done with experimental metal cored filler wire under the condition in **Table 4**. The specimen was left as it for two days after the test welding.

Table 4 Conditions used in the modified Navy-Torture cracking test.

Welding parameter:	GTA weld
	DCEN, 180A, 17V
	Welding speed 100mm/min.
	Heat input 1.8kJ/cm
	Arc length 3mm
Electrode:	EWTh-2, 4mm dia.
Shielding gas:	pure Ar (20litre/min.)
Back shielding gas:	pure Ar (10litre/min.)

The macroscopic feature of fracture surface of the modified Navy-Torture cracking test specimen was observed with the naked eye, and then the microscopic feature was observed in detail with SEM. As mentioned later, the SEM observation revealed solidification cracking region, sub-solidus cracking region consisting of intergranular fracture region (IG_C) and artificially fractured region consisting of dimple or cleavage fracture region (C), and each fracture region shows its macroscopically peculiar feature which can be discriminated on a light fractograph of about X10 magnification. Therefore, the area fraction of each fracture region occupied in the whole of the fracture surface was measured with a planimeter on the light fractograph. In this study, the solidification crack ratio (C_R^F) was used as an index of a practical cracking propensity. Moreover, the length of solidification crack on the welded bead surface was measured by binocular microscope, and the crack ratio(C_R^L), where C_R^L = total solidification crack length/ the whole bead length, was used to evaluate the practical cracking tendency.

2.3 Microsegregation of impurity elements

It is presumed that the area fraction or roughly the number of interdendritic inclusions enriched with P and S implys the degree of interdendritic microsegregation of P and S during weld solidification. Therefore, the microsegregation of P and S was evaluated by number of such inclusions in weld metals which were water-quenched during GTA welding. Moreover, the shapes, main constituting elements, structure types and distribution profiles were measured. Inclusions were identified by using conventional carbon-extraction replicas with the aid of transmission electron microscope(TEM), energy dispersive X-ray spectrometer(EDX) and partly wave dispersive X-ray spectrometer(WDX) for O and S with SEM. The constituents in inclusion were measured with SEM observation and EDX at X 3000 magnification.

2.4 Liquation temperature of grain-boundary

The melting temperature of grain-boundary was directly measured by hot-stage microscope on heating cycle in order to compare it with the lower temperature limit of the BTR.

The specimen used was cut off from the weld metal which was water-quenched, and machined to the shape shown in **Fig. 5**. As-polished specimen was heated by direct current with A.C. in hot-stage microscope, which was initially evacuated to 1×10^{-4} Torr and filled with argon gas to one atmosphere. The heating rate selected was about 20°C/sec.

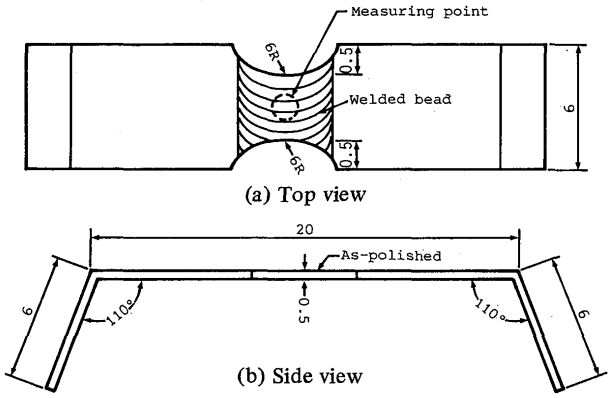

Fig. 5 The shape and dimensions of the specimen used for hot-stage microscope.

3. Experimental Results and Discussions

3.1 Correlation between ferrite content at room temperature and solidification crack susceptibility

Figure 6 shows the typical appearances of cracks by the Trans-Verestraint cracking test. Two types of hot cracks occurred in weld metals of ferrite content = 1% and 99%, that is to say, one is solidification crack and the other is ductility-dip crack at the lower temperature.[12] On the other hand, in the cases of ferrite content = 6% and 44%, rather smaller solidification cracks occurred but no ductility-dip crack occurred. **Figure 7** shows the range of solidification cracks and ductility-dip cracks along the weld line. The abscissa and the ordinate indicate the ferrite content and the distance from solidification front, respectively. It is understood that both solidification cracks and ductility-dip cracks occurred when ferrite content less than 1% or more than 80%. However, no ductility-dip crack occurred when ferrite content is in the range from 3 to 80%. It is noticed that no ductility-dip

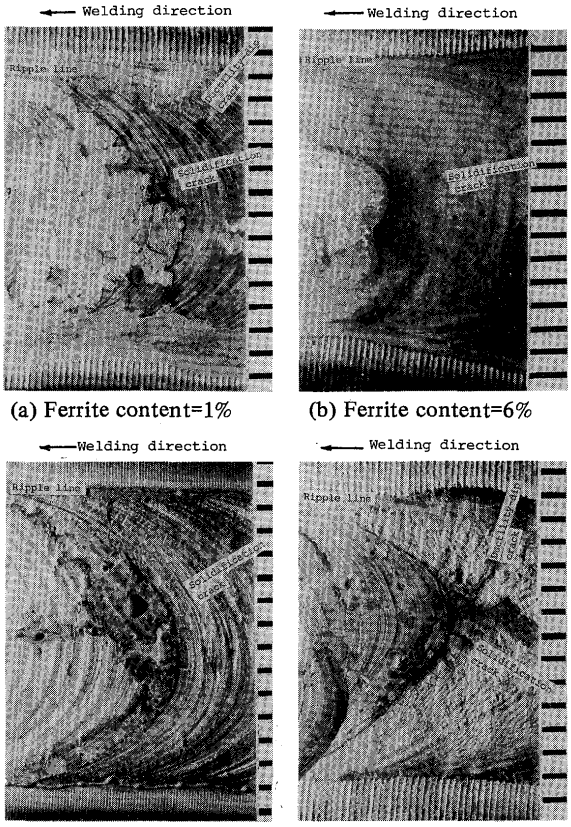

(a) Ferrite content=1% (b) Ferrite content=6%

(c) Ferrite content=44% (d) Ferrite content=99%

Fig. 6 Typical cracks in weld metals after the Trans-Varestraint cracking test.

crack was observed in SUS 430 and SUS $329J_2L$ base metals in spite of their ferrite content more than 80%.

Since solidification cracking is considered to be the more serious problem of these hot cracks,[6] solidification cracking is mentioned hereafter in detail. **Figure 8** shows the relationship between ferrite content and maximum crack length, total crack length, where open mark means experimental deposited metals and solid mark does commercial base metals. This figure indicates the clear minimum in solidification crack susceptibility at a ferrite level of 5 to 20%. As ferrite content decreases below 5%, the susceptibility increases rapidly. Similarly as ferrite content increases above 20%, the susceptibility increases gradually. This result agrees well with Kujanpää's results.[2–4]

Moreover, the susceptibility was roughly independent of the Cr_{eq} values, as seen from the comparison of different marks (△, ○, ◇) at the same ferrite level. On the other hand, the susceptibilities of commercial base metals marked by (♦) are slightly lower than that of experimental deposited metals. The reason of the difference in the susceptibility is not clear at the present.

Subsequently, the modified Navy-Torture cracking test was done and **Fig. 9** shows the surface appearances of tested weld beads, where longitudinal crack was seen in the cases of ferrite content = 1% and 99%. As mentioned later, only solidification cracking occurred in the former

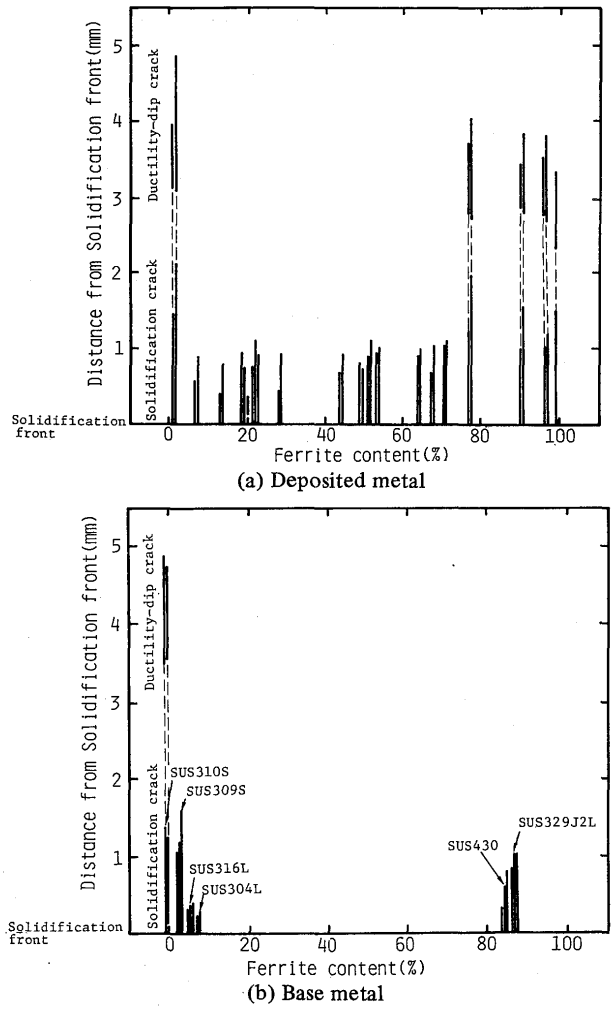

(a) Deposited metal

(b) Base metal

Fig. 7 Relation between ferrite content and regions of solidification cracks and ductility-dip cracks.

case and both solidification and sub-solidus cracking occurred in the latter case. In the case of ferrite content = 44%, solidification cracking occurred only at crater part. Moreover, it was noticed that no crack was observed in the case of ferrite content = 6%. **Figure 10** shows the macrographs and their sketches of their artificially fractured surfaces, where the fracture surface is classified into four regions according to the typical microfractographs shown in **Fig. 11**. The Types D and D-F are the characteristics of solidification cracking.[8] The Type IG_C is subsolidus cracking. Now the authors have expressed here as sub-solidus crack because this crack is not cleared yet whether ductility-dip crack or cold crack due to hydrogen. The authors, however, imagine it to be cold cracking judging from its microscopie feature.[13] The Type C was maybe formed together with dimple by the artificial fracturing. Thus, C_R^F was measured as the ratio of the area of Types D and D-F over whole area. **Figure 12** shows the relation between ferrite content and the crack ratios C_R^F and C_R^L, and means that the crack tendency agrees well that evaluated by the Trans-Verestraint test.

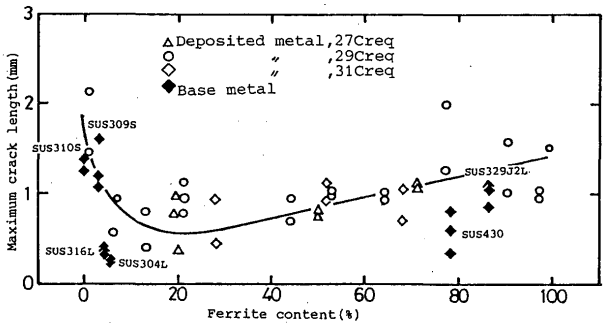

(a) Maximum crack length vs. ferrite content.

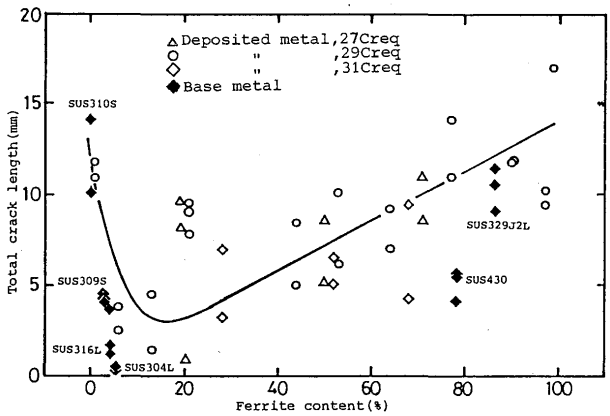

(b) Total crack length vs. ferrite content.

Fig. 8 Relation between ferrite content, maximum crack length and total crack length in the Trans-Varestraint test.

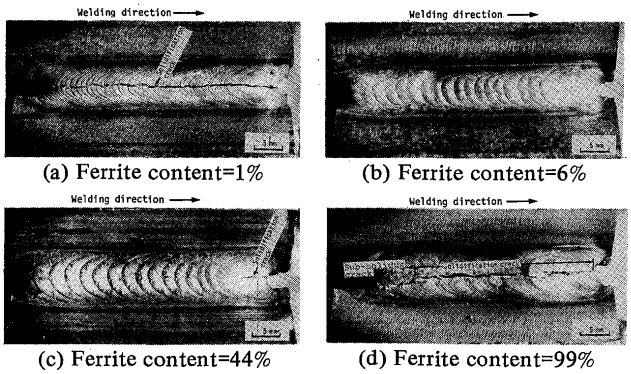

(a) Ferrite content=1% (b) Ferrite content=6%

(c) Ferrite content=44% (d) Ferrite content=99%

Fig. 9 Typical cracks in weld metals after the modified Navy-Torture cracking test.

3.2 Microsegregation of impurity elements

3.2.1 Identification of inclusions

Figure 13 shows the SEM microstructure near the solidification front in weld metal of ferrite content = 1%, the EDX result of typical inclusions, their diffraction patterns and their key-diagrams, where Cu peak came from Cu mesh and/or Cu mesh-holder. The microstructure shows that granular and rod-like shaped inclusions identified as FeS type sulphide containing a high amount of Cr existed at cellular dendritic boundary and columnar grain-boundary. In the case of ferrite content = 44%, as shown in **Fig. 14**, globular shaped inclusions identified as

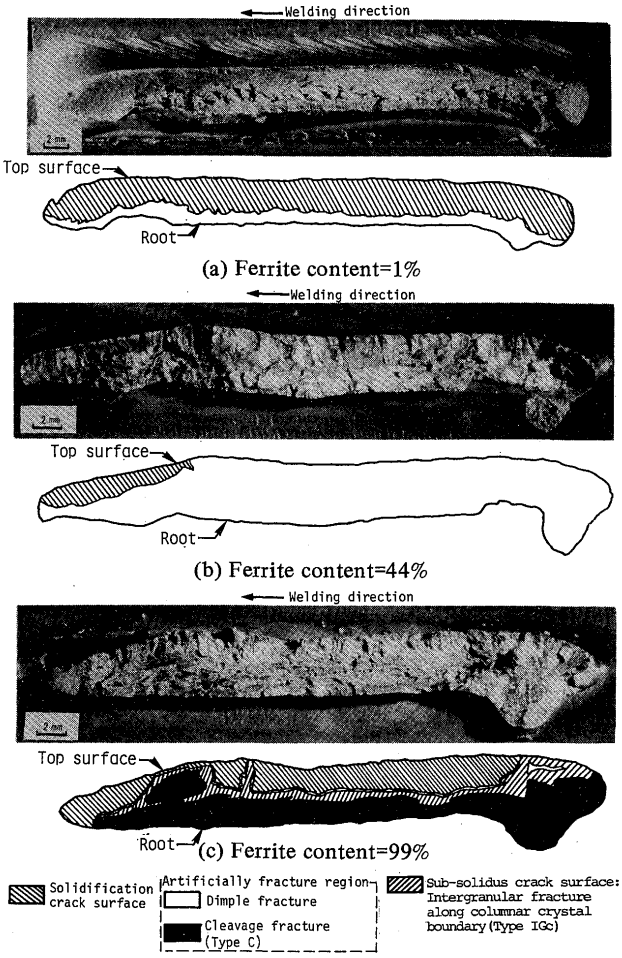

Fig. 10 Light fractographs after the modified Navy-Torture cracking test.

silicate type oxide containing a high amount of Mn and a little amount of S existed on Widmanstätten austenite phases corresponding to solidification grain-boundaries. In the case of ferrite content = 99%, as shown in **Fig. 15**, two types of inclusions coexisted, that is to say, one is identified as Cr_2O_3-Fe_2O_3 type complex oxide containing a high amount of S and another is globular silicate type oxide like that mentioned in Fig. 14. Moreover, the former existed along cellular dendritic boundary and columnar grain-boundary, and the latter existed inside cellular dendrite.

Figure 16 shows the main constituting elements in the inclusions above mentioned together with those of SUS 310S base metal for comparison. In the case of ferrite content = 1%, as already mentioned, the inclusions identified as FeS type sulphide containing a high amount of S and such transient metals as Fe, Cr, Ni except for Mn, and an appreciable amount of P etc. By the way, it is well known[11] that α-MnS type sulphide is frequently detected in commercial stainless steel base metals solidified as primary austenite. However, α-MnS type sulphide was not detected in experimental deposited metals in spite of the same level of Mn contents as commercial stainless

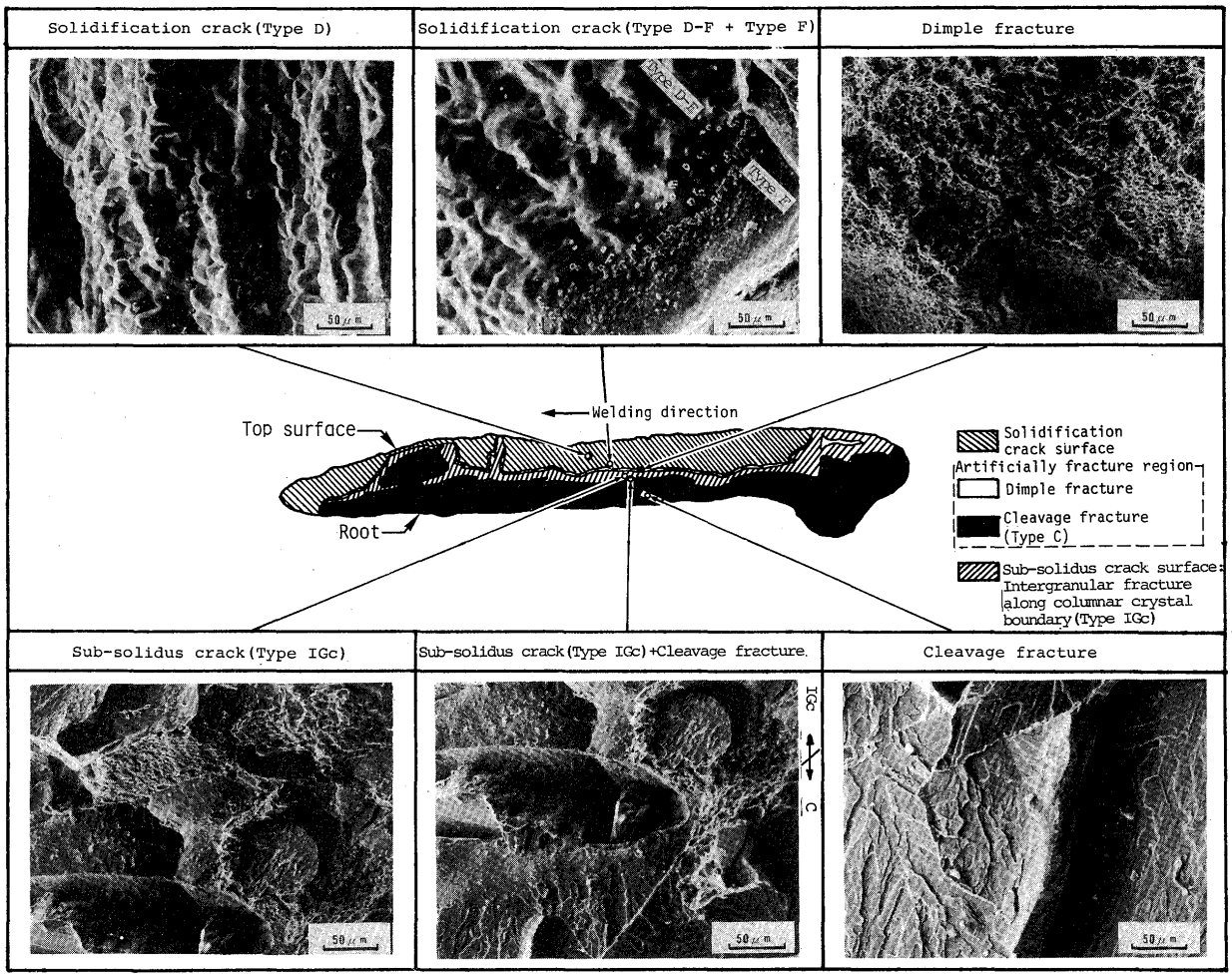

Fig. 11 SEM fractographs after the modified Navy-Torture cracking test, ferrite content = 99%.

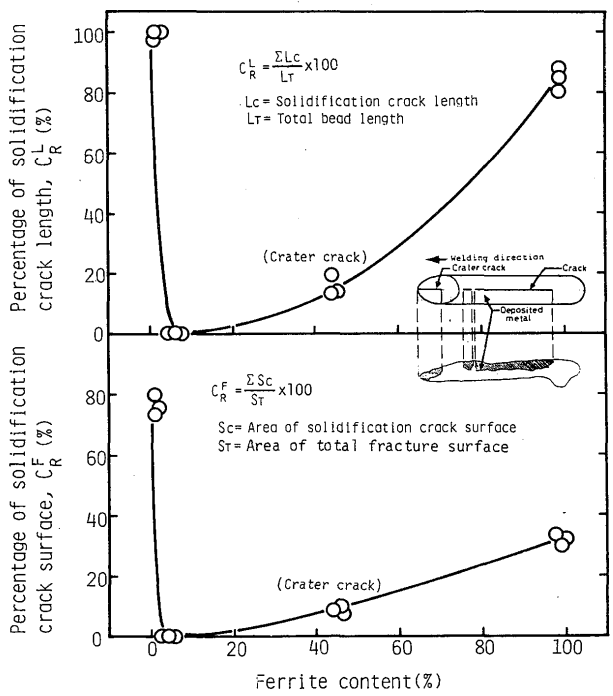

Fig. 12 Relation between ferrite content and crack ratios C_R^F, C_R^L in the modified Navy-Torture cracking test.

steel base metals. The reason of this discrepancy is considered that O level of experimental deposited metals is fairly higher due to welding than that of commercial ones and Mn has a much more potent tendency to combine O than S as well known, and thus Mn content in the matrix to combine S decreased because of forming MnO type oxide. In the cases of ferrite content = 6% and 44%, the inclusions identified as silicate type oxide contained mainly Si, Mn and O, but neither sulphide nor phosphide was detected. In the case of ferrite content = 99%, the two types of inclusions coexisted as above mentioned. Inclusion identified as the complex oxide contained much S, Cr, Fe, O and an appreciable P. Another inclusion identified as silicate type oxide was similar to those in the cases of ferrite content = 6% and 44%. Namely, neither sulphide nor phosphide was detected in this case. On the other hand, in the case of SUS 310S base metal, Cr_3P type phosphide was mainly detected, but sulphide was rarely detected because of low S content (see Table 2).

3.2.2 Amounts of inclusions as a measure of micro-segregation

Figure 17 shows the relationship between ferrite content and the number of inclusions enriched with P and

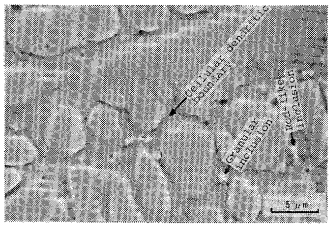

(a) SEM microstructure

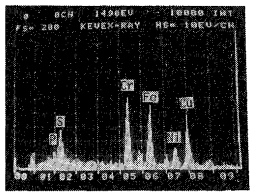

(b) EDX result for typical inclusion

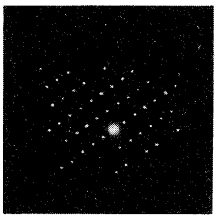

(c) Electron diffraction pattern-(1)

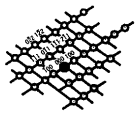

Beam // FeS (01 1)

(d) Key-diagram-(1)

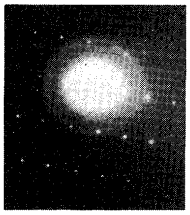

(e) Electron diffraction pattern-(2)

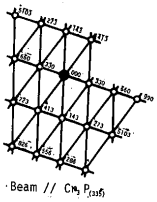

Beam // Cr_3P (335)

(f) Key-diagram-(2)

Fig. 13 SEM microstructure of weld metal (a), EDX result (b), electron diffraction pattern (c) and (e), and key-diagram (d) and (f) for typical inclusion in the case of ferrite content=1% indicating formation of FeS type sulphide and partially Cr_3P type phosphide.

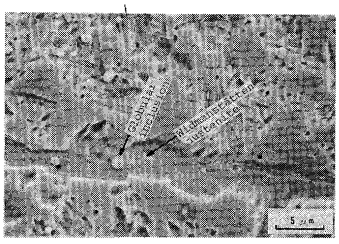

(a) SEM microstructure

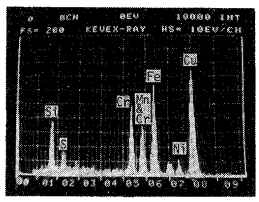

(b) EDX result for typical inclusion

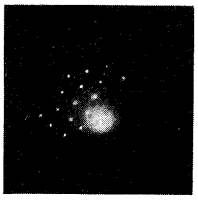

(c) Electron diffraction pattern

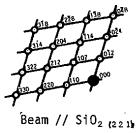

Beam // SiO_2 (221)

(d) Key-diagram

Fig. 14 SEM microstructure of weld metal (a), EDX result (b), electron diffraction pattern (c) and key-diagram (d) for typical inclusion in the case of ferrite content=44%, indicating formation of silicate type oxide containing a little amount of S.

S in weld metals near the solidification front water-quenched. The open mark indicates the inclusions enriched with P, hatching mark does those enriched with S and solid mark does those enriched with both P and S. This figure gives the clear minimum in the number of inclusions at a ferrite level of 6 to 20%. As ferrite content decreased, the number of inclusions increased rapidly. As

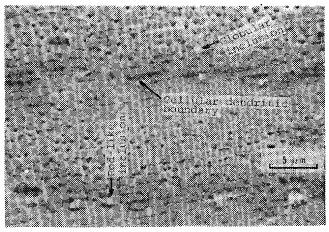

(a) SEM microstructure

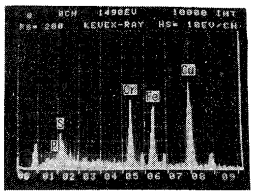

(b) EDX result for typical inclusion

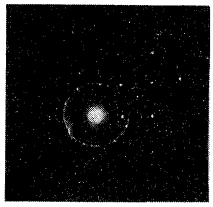

(c) Electron diffraction pattern-(1)

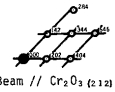

Beam // Cr_2O_3 (212)

(d) Key-diagram-(1)

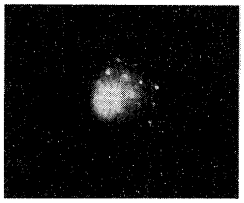

(e) Electron diffraction pattern-(2)

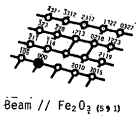

Beam // Fe_2O_3 (591)

(f) Key-diagram-(2)

Fig. 15 SEM microstructure of weld metal (a), EDX result (b), electron diffraction pattern (c) and (e), and key-diagram (d) and (f) for typical inclusion in the case of ferrite content=99%, indicating formation of Cr_2O_3-Fe_2O_3 complex oxide containing a high amount of S.

ferrite content increased, the number of inclusions increased gradually. This tendency was commonly observed in deposited metals and base metals as seen in (a) and (b). In general, the number of inclusions enriched with P was commonly slight in deposited metals.

3.2.3 Distribution profiles of inclusions

Figure 18 shows the distribution profiles of inclusions along solidification grain-boundary from the liquidus temperature to the lower temperature limits of the BTR in the weld metals, which were water-quenched during GTA welding. The abscissa and the ordinate indicate quenching temperature and the number of inclusions enriched with P and/or S, respectively. Moreover, each mark has the same meaning as that in Fig. 17. In the case of ferrite content = 1%, the number of inclusions is very large in the full range from the liquidus temperature to the lower temperature limit of the BTR, and have a peak at about 20 to 30°C below the liquidus temperature. This peak is probably because of the balance between the concentration of impurities due to microsegregation during solidification and the loss due to diffusion to the matrix. Compared with other results mentioned later, it is deduced that the degree of microsegregation of P and S is large in the full range of temperature. On the other hand, in the case of ferrite content = 6%, it is clear that the degree of microsegregation of P and S is slight in the full range of

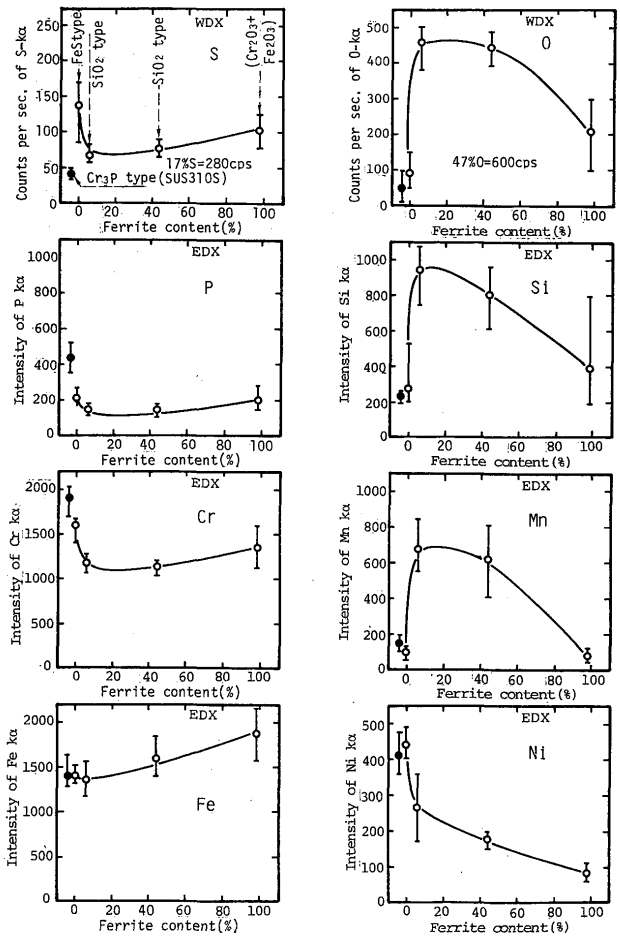

Fig. 16 Effect of ferrite content on constituents of inclusions, referenced inclusion in SUS 310S base metal is marked by (↓).

the BTR. This exception is considered as below. Its solidification process consists of probably the primary ferrite and subsequent eutectic ferrite-austenite solidification (including divorced eutectic ferrite or partly peritectic solidification).[14] When the ferrite grows as the primary phase during solidification, it is able to dissolve larger amounts of P and S owing to the large solubility thus lower the segregation of these elements. Besides, the authors guess that the eutectic reaction gives some effects on decreasing the segregation of these elements. On the other hand, in the cases of ferrite content = 44% and 99%, it is noticed that the degree of microsegregation of the elements is large in the higher temperature range, but in the lower temperature range as small as that in the case of ferrite content = 6%. In these cases, the number of inclusions enriched with P is less than that of ferrite content = 1%. Moreover, the declining slopes of distribution curves of ferrite content = 44% and 99% are steeper than that of ferrite content = 1%. This tendency may be explained by the large solubility and diffusibility of the elements in ferrite phase.

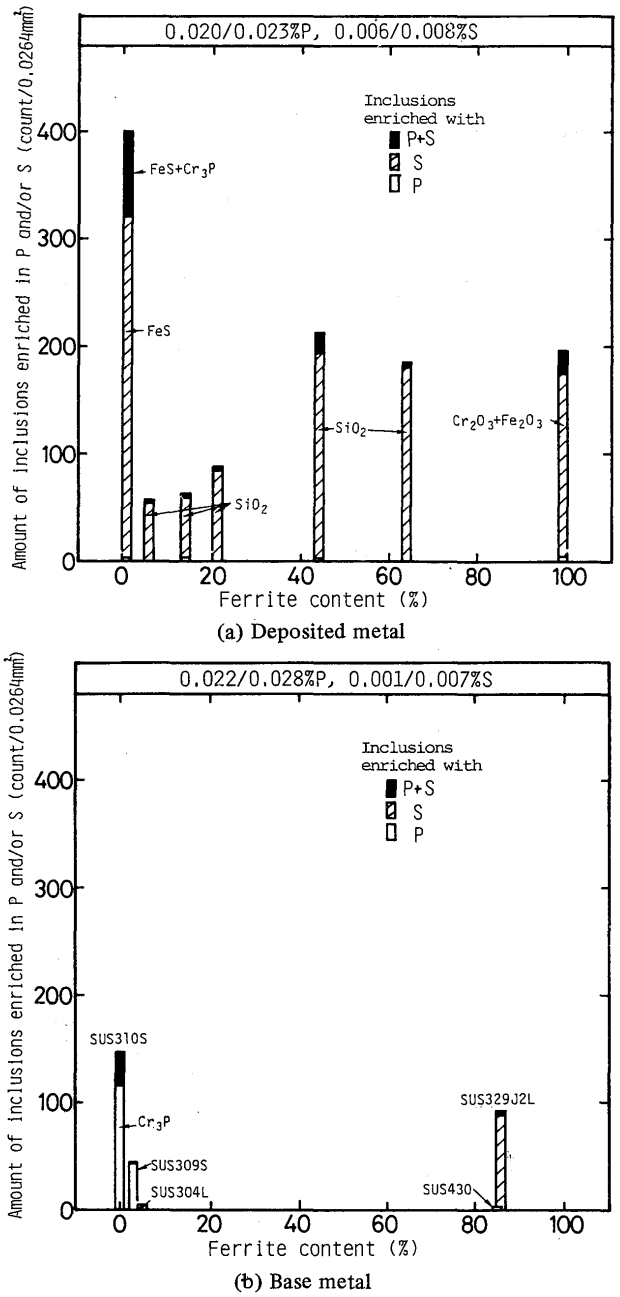

Fig. 17 Relation between ferrite content and number of inclusions enriched with P and/or S.

3.3 Liquation temperature of grain-boundary and their influence on solidification crack susceptibility

Figure 19 shows a thermally etched microstructure of the specimen rapidly heated to a peak temperature of about 1245°C and its sketch in the case of ferrite content = 1%. It is obvious that liquation occurred at the tripple point of grain-boundaries and liquid phase was about to penetrate into grain-boundaries. Subsequently, the BTR, the liquidus, the nominal solidus and the liquation temperatures are plotted vs. Ni content in **Fig. 20**, constructing a pseudo phase diagram in a sense, where the

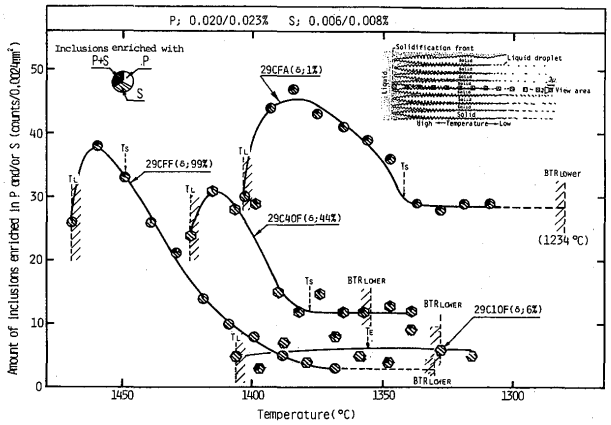

(a) Deposited metal

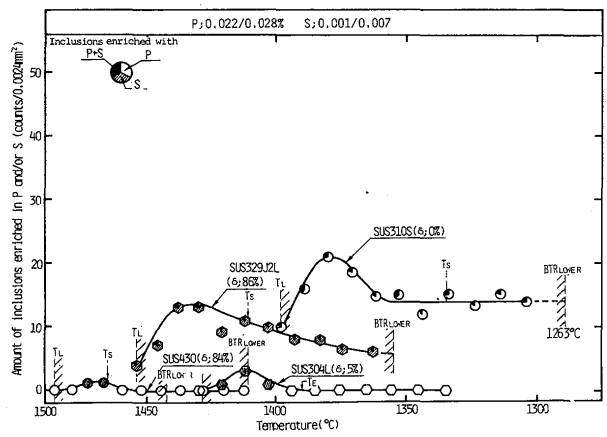

(b) Base metal

Fig. 18 Distribution profile of inclusions enriched with P and/or S within the BTR.

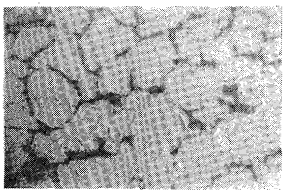

(a) Thermally etched microstructure

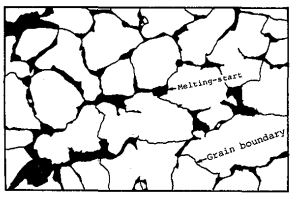

(b) Schematic representation of (a)

Fig. 19 Thermally etched microstructure heated to a peak temperature about 1245°C, showing partial melting of grain-boundary, ferrite content=1%.

designations of solidification process are the same as those in Table 5 mentioned later. It is noticed in the cases of ferrite content = 1% and 99% that the liquation temperatures were fairly lower than the nominal solidus temperature and near the lower temperature limits of the BTR. Therefore, it may be presumed that deposited metals of ferrite content = 1% and 99% have a high susceptibility to solidification cracking due to lowered true solidus caused by enhanced microsegregation. On the contrary, in the cases of ferrite content = 6% and 44%, the liquation temperatures were slightly lower than the nominal solidus temperature and near the lower temperature limits of the BTR. Thus, the liquation temperature agrees well with the lower temperature limits of the BTR. Namely, the lower

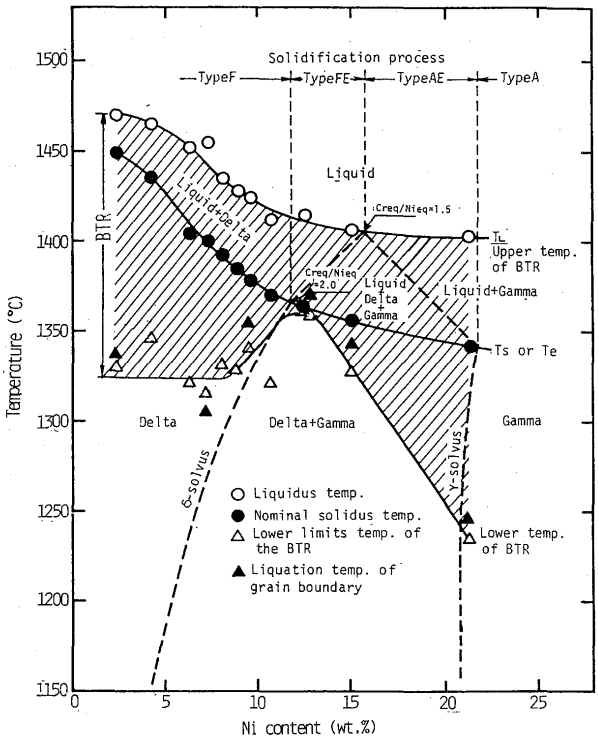

Fig. 20 Relation among the BTR, liquidus, nominal solidus and liquation temperature of grain-boundary.

the liquation temperature is, the higher solidification crack susceptibility is.

3.4 Fractographic feature of solidification crack in the Trans-Varestraint cracking test

As shown in **Fig. 21**, the cracked surfaces of ferrite content=1% and 99% give a feature composed of dendritic Type D, transient Type D-F and flat Type F.[7] These are reflected by the simple solidification mode of single phase in spite of the difference in primary phase. On the other hand, the cracked surface of ferrite content = 6% gives a feature composed of only Type D. A detailed study has revealed[8] that this feature is related partly to the morphology of cellular dendrites and partly to the eutectic reaction during weld solidification. **Figure 22** shows the relationship between ferrite content and area fraction of Type F over the whole cracked surface. This figure indicates the clear minimum in area fraction of Type F at ferrite levels of 6% and 13%. As ferrite content decreased, the fraction area increased rapidly. As ferrite content increased, the fraction area increased gradually. This tendency is the same as the relationship between ferrite content and solidification crack susceptibility. Consequently, it is understood that the susceptibility connects with area fraction of Type F fracture surface. The cause of this result is inferred mainly that such impurities as P, S and O remarkably extend the solidification temperature range to form phosphide, sulphide and oxide containing much S of low melting point at the last stage of

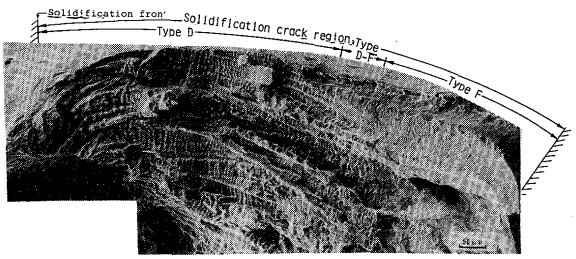

(a) Ferrite content=1%

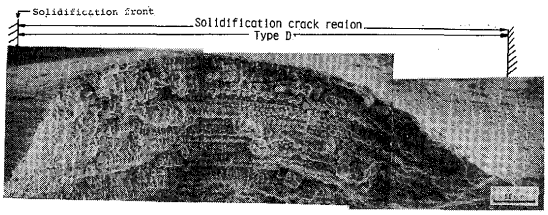

(b) Ferrite content=6%

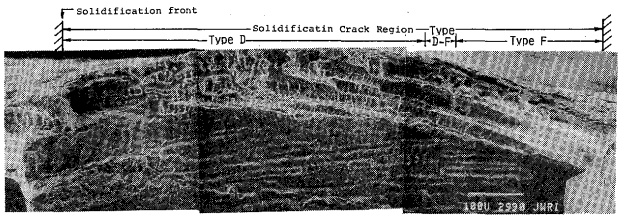

(c) Ferrite content=99%

Fig. 21 Effect of ferrite content on SEM microfractograph of solidification cracking.

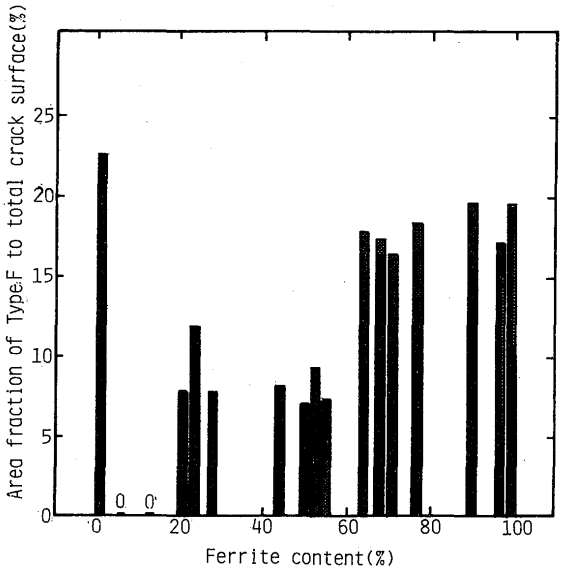

Fig. 22 Relation between ferrite content and area fraction of Type F fracture surface in total crack surface.

solidification correspond to Type F region[8].

All the results shown in Figs. 13 to 22 suggest that the microsegregation in high ferrite level is unexpectedly fairly high compared with that in ferrite level of 5 to 20% and that the degree of interdendritic microsegregation has intimate correlation with solidification cracking. Of course, the microsegregation is the highest in full austenite region, but the number and the constituents of inclusions near the solidification front water-quenched strongly claim that the microsegregation in high ferrite level is very high to an extent slightly lower than that in full austenite region. This was confirmed by not only the behavior of inclusions but also the area fraction of Type F fracture surface reflecting the degree of remaining minute residual liquid phase enriched with impurities at the last stage of solidification. As an interesting difference from full austenite region in which sulphide and phosphide were detected, neither sulphide nor phosphide was detected in spite of the enrichment of a high amount of S and a little amount of P into inclusions. Rather, only several types of oxides were detected. It is estimated that S and P were contained into oxides. Therefore, it may be imagined that the reason of high susceptibility in high ferrite level is the lowered eutectic temperature of the matrix and the oxides enriched with S and P as imagined from the liquation temperature of grain-boundary. Another interesting phenomena concerning the microsegregation in high ferrite level are that P segregation is fairly little compared that in full austenite region and that water-quenching was necessary to find out its relatively high microsegregation of impurities. Both of them may be explained from the fact that ferrite phase has high solubility and diffusibility of such impurities as S and P. The reason of the high microsegregation in high ferrite level is not clear at the present.

3.5 Effects of grain size and solidification mode on solidification crack susceptibility

Since solidification cracking occurs during weld solidification, it is important to know the solidification mode. For this purpose, the location of crack in the microstructure at RT and weld solidification structure, which was water-quenched during GTA welding, were observed by using optical microscope. Both the microstructure at RT near the solidification crack and the weld solidification structure near the solidification front in the case of ferrite content = 1% shown in **Fig. 23**, and ferrite content = 99% in **Fig. 24**, in which the susceptibilities were high, indicate that the solidification cracks occurred and propagated linearly along a coarse columnar crystal boundary. On the other hand, in the case of ferrite content =44% shown in **Fig. 25**, it is noticed that solidification crack passes in jigzag mode through a several small equiaxed crystal boundaries. The same phenomena were observed in the ferrite range from 20 to 70%, and it would be difficult for cracks to propagate. **Figure 26** shows the relationship between ferrite content and grain size in solidification structure near the solidification front. It is obvious that the grain size in longitudinal direction was varied with ferrite content, that is, the columnar crystal had a tendency to grow in longitudinal direction in case of ferrite content less than 20% or more than 70%, but rather

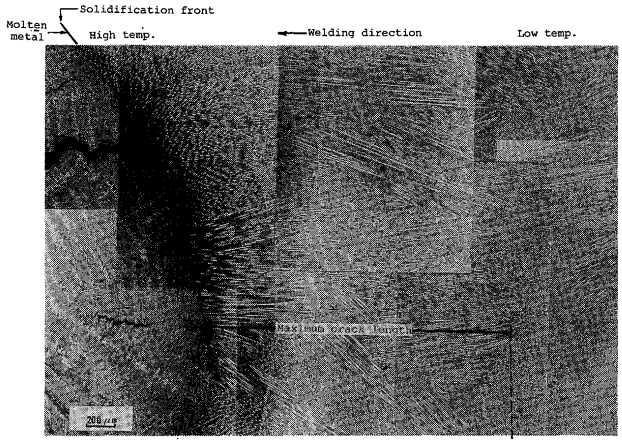

(a) Water-quenched microstructure near the solidification front

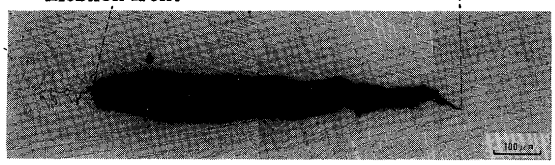

(b) Solidification crack

Fig. 23 Solidification microstructure and crack, ferrite content = 1%.

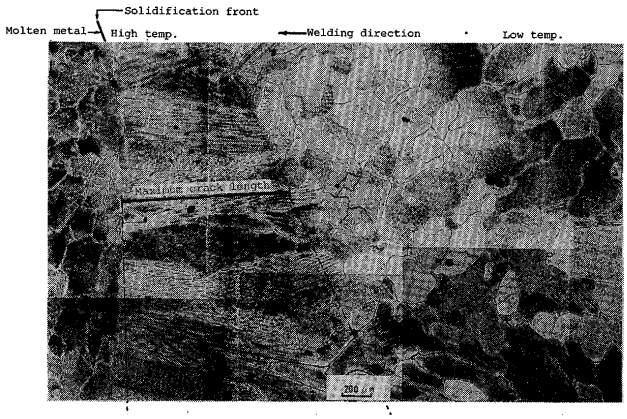

(a) Water-quenched microstructure near the solidification front

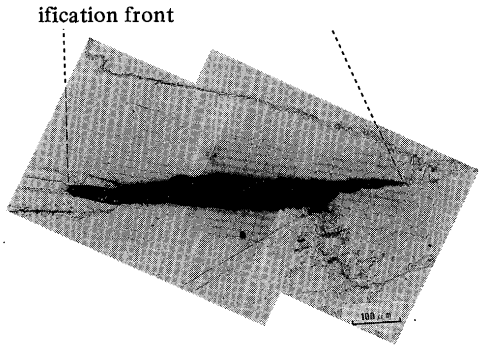

(b) Solidification crack

Fig. 24 Solidification microstructure and crack, ferrite content=99%.

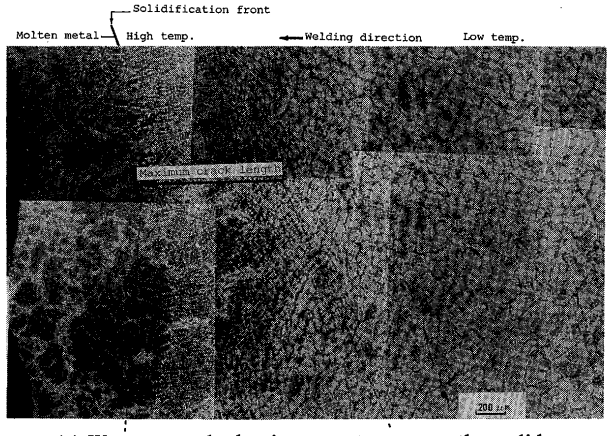

(a) Water-quenched microstructure near the solidification front

(b) Solidification crack

Fig. 25 Solidification microstructure and crack, ferrite content=44%.

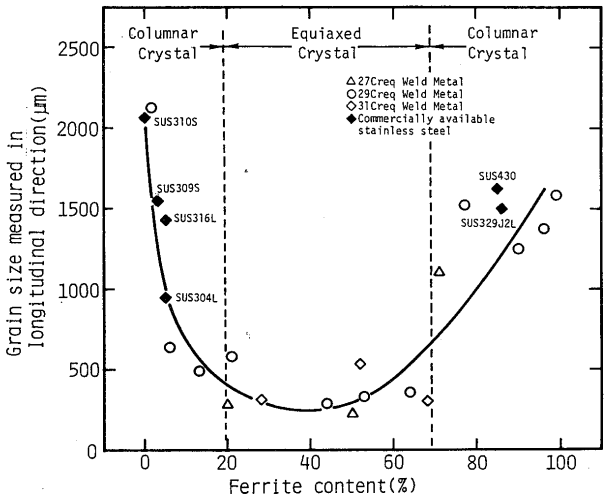

(a) Longitudinal direction

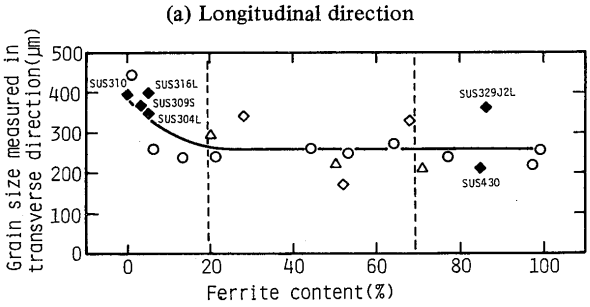

(b) Transverse direction

Fig. 26 Relation between ferrite content and grain size during weld solidification.

equiaxed crystals were formed in the ferrite range from 20 to 70% and thus grain size in longitudinal direction was relatively small. Comparing Figs. 8 and 12 with Fig. 26, the ferrite level which gave the minimum grain size, however, deviate a little from that giving the minimum crack susceptibility. Therefore, the effect of grain size on the susceptibility may be subsidiary to that of the microsegregation. Microscopic observation suggests that this

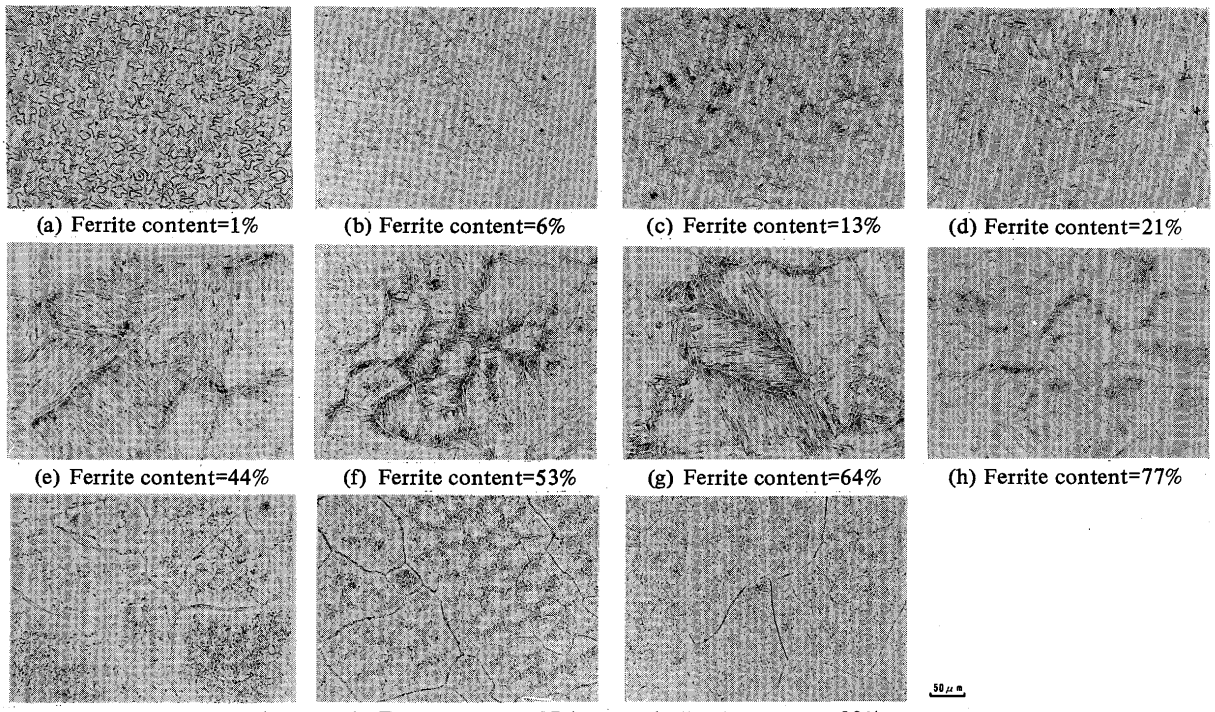

(a) Ferrite content=1% (b) Ferrite content=6% (c) Ferrite content=13% (d) Ferrite content=21%

(e) Ferrite content=44% (f) Ferrite content=53% (g) Ferrite content=64% (h) Ferrite content=77%

(i) Ferrite content=90% (j) Ferrite content=97% (k) Ferrite content=99%

Fig. 27 Microstructures of weld metals at room temperature (top surface, electrolytic etching at 4V in 10% oxialic acid)

tendency of grain size is affected by the solidification mode mentioned next, but the mechanism is not clear at the present.

Then, the solidification process of each materials used were presumed by the characteristic microstructure at RT and Cr_{eq}/Ni_{eq} ratios. As-welded microstructures were carefully observed on the basis of the classification by Katayama et al.[14] **Figure 27** shows these microstructures. On the other hand, Suutala et al. found out that solidification process depends on the weld metal composition. Namely, the weld metal solidifies as primary austenite under Cr_{eq}/Ni_{eq} ratio less than 1.5, as primary ferrite and eutectic austenite-ferrite under Cr_{eq}/Ni_{eq} ratio from 1.5 to 2.0, and as single ferrite under Cr_{eq}/Ni_{eq} ratio more than 2.0. The solidification processes predicted from both microstructure and Cr_{eq}/Ni_{eq} ratio are tabulated in **Table 5** and it is seen that these solidification processes agree well each other.

All the main metallurgical factors affecting the crack susceptibility are illustrated in **Fig. 28.** As ferrite content is increased, solidification mode changes from Type A to AE, FE and F, accompanied with the concave behavior of degree of interdendritic microsegregation of such impurities as S and P showing the minimum at Type FE, namely at ferrite level of 5 to 20%. This behavior of microsegregation causes the similar behavior of solidification temperature range ($\triangle T_{liquidus\text{-}true\ solidus}$) corresponding to brittleness temperature range (BTR). On the other hand, also grain size has similar concave behavior vs. ferrite content, although the minimum point deviates a little from that of the susceptibility, and thus maybe have subsidiary effect on the crack. As the results of all these factors, the crack susceptibility changes as shown in the lowest part in Fig. 28. That is, the susceptibility is minimum at Type FE, namely at ferrite level of 5 to 20%, and is very high in not only full austenite region (Type A) but also 80 to 100% ferrite region (upper region of Type F).

Table 5 Relation between microstructure and solidification mode.

Materials (Mark)	Katayama			Suutala	
	Characteristic microstructure (Mode)	Solidification process (Type)		Creq/Nieq	Solidification process (Type)
29CFA	IF	AE	$L\to L+\gamma\to L+\gamma+\delta\to\gamma+\delta$	1.14	A or AE
29C10F	VF	FE	$L\to L+\delta\to L+\delta+\gamma\to\delta+\gamma$	1.52	FE
29C20F	VF+LF	FE	〃	1.81	FE
29C30F	AF	F	$L\to L+\delta\to\delta\to\delta+\gamma$ (with $\delta\to\gamma$ trans.)	2.04	F
29C40F	WA	F	〃	2.21	F
29C50F	WA	F	〃	2.33	F
29C60F	WA	F	〃	2.45	F
29C70F	WA	F	〃	2.66	F
29C80F	WA	F	〃	2.86	F
29C90F	WA	F	〃	3.74	F
29CFF	WA	F	〃	4.95	F
27C30F	WA	F	$L\to L+\delta\to\delta\to\delta+\gamma$ (with $\delta\to\gamma$ trans.)	2.09	F
27C50F	WA	F	〃	2.46	F
27C70F	WA	F	〃	2.67	F
31C30F	WA	F	$L\to L+\delta\to\delta\to\delta+\gamma$ (with $\delta\to\gamma$ trans.)	1.98	F
31C50F	WA	F	〃	2.23	F
31C70F	WA	F	〃	2.59	F
SUS310S	FA	A	$L\to L+\gamma\to\gamma$	1.19	A or AE
SUS304L	VF	FE	$L\to L+\delta\to L+\delta+\gamma\to\delta+\gamma$	1.83	FE
SUS316L	VF	FE	〃	1.54	FE
SUS309S	VF+LF	FE	〃	1.63	FE
SUS329J2L	WA	F	$L\to L+\delta\to\delta\to\delta+\gamma$ (with $\delta\to\gamma$ trans.)	2.68	F
SUS430	—	—	—	9.80	F

Characteristic microstructure
IF:Intercellular eutectic ferrite
VF:Vermicular(dendritic or skeletal)ferrite
LF:Lacy ferrite
AF:Acicular(lathy)ferrite
WA:Widmanstätten(feathery)austenite

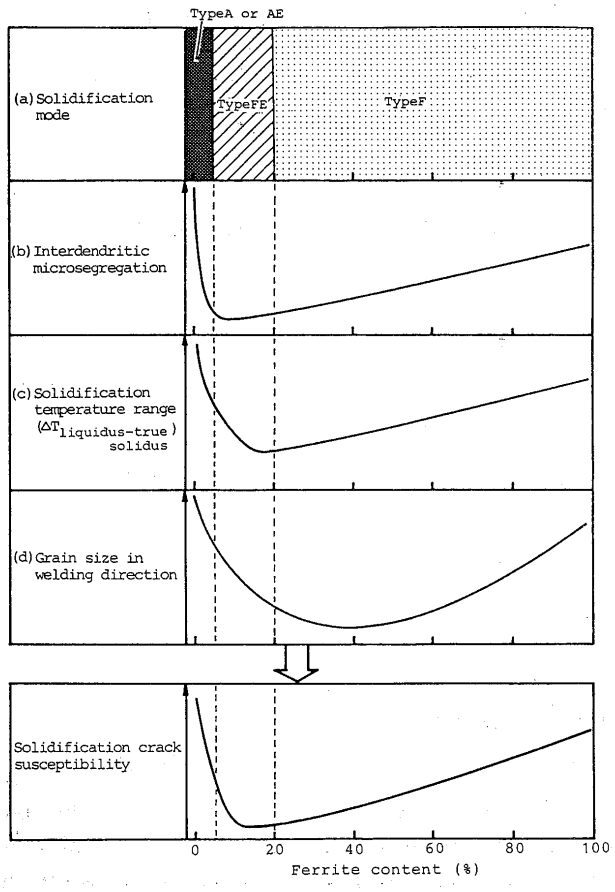

Fig. 28 Summarized illustration of effects of main metallurgical factors on solidification crack susceptibility vs. ferrite content.

4. Conclusion

Metallurgical characteristics in weld metals such as microsegregation of impurity elements, feature of cracking surfaces and microstructure were observed in order to study the effects of ferrite content on solidification crack susceptibility in deposited weld metals of duplex austenitic-ferritic stainless steels.

Main conclusions obtained are as follows.

1) Both Trans-Varestraint cracking test and the modified Navy-Torture cracking test as a practical hot cracking test gave a similar crack susceptibility vs. ferrite level. Namely, the susceptibility was minimum at a ferrite level from 5 to 20%, and was high in not only near full austenite region but also 80 to 100% ferrite region.
2) Number and constituents of interdendritic inclusions just behind the solidification front, the distribution profile of the number and the constituents of interdendritic inclusion along the distance from the solidification front, the liquation temperature of grain-boundary, all these suggest with one accord that interdendritic microsegregation is enhanced in high ferrite level compared with 5 to 20% ferrite level, although the microsegregation is the highest in full austenite region. This is also supported by fractographic feature of solidification crack. This behavior of the microsegregation causing solidification temperature range is the main reason of the crack susceptibility above mentioned.
3) As impurities S is frequently, but P is rarely detected, although there was neither sulphide nor phosphide in any ferrite level except for full austenite region. Therefore, it was guessed that S and a little amount of P were contained in oxides.
4) Grain size has nearly similar tendency to the crack susceptibility vs. ferrite level. Therefore, grain size maybe another contributing factor to the crack.

References

1) J.W. Puph, et al.: Trans. AIME, 188 (1950), 269.
2) V. Kujanpää, et al.: Welding Research International, Vol. 9 (1979), No. 2, 55–76.
3) V. Kujanpää, et al.: Metal Const. (1980), No. 6, 282–285.
4) V. Kujanpää, et al.: Metal Const. (1985), No. 1, 40R–46R.
5) J.C. Borland, et al.: British Welding J., 7 (1960), No. 1, 22–59.
6) J. Honeycombe, et al.: Metal Const. and British Welding J., 2 (1970), No. 9, 375–380.
7) F. Matsuda and H. Nakagawa: Trans. of JWRI, Vol. 8 (1979) No. 1, 155–157.
8) F. Matsuda, H. Nakagawa, S. Ogata and S. Katayama: Trans. of JWRI, Vol. 7 (1978), No. 1, 59–70.
9) F. Matsuda, H. Nakagawa, T. Uehara, S. Katayama and Y. Arata: Trans. of JWRI, Vol. 8 (1979), No. 1, 105–112.
10) T. Senda and F. Matsuda: Trans. of JWRI, Vol. 2 (1971), No. 2, 1–22.
11) F. Matsuda, S. Katayama and Y. Arata: Trans. of JWRI, Vol. 10 (1981), No. 2, 73–84.
12) Y. Arata, F. Matsuda and S. Katayama: Trans. of JWRI, Vol. 6 (1977), No. 1, 105–116.
13) F. Matsuda, H. Nakagawa, K. Shinozaki, et al.: Trans. of JWRI, Vol. 6 (1977), No. 2, 59–73.
14) S. Katayama, T. Fujimoto and A. Matsunawa: Trans. of JWRI, Vol. 14 (1985), No. 1, 123–137.
15) N. Suutala, T. Takalo and T. Moisio: Metall. Trans., Vol. 10A (1979), No. 4, 512–514.
16) T. Takalo, N. Suutala and T. Moisio: Metall. Trans., Vol. 10A (1979), No. 8, 1173–1181.
17) N. Suutala, T. Takalo and T. Moisio: Metall. Trans., Vol. 10A (1979), No. 8, 1183–1190.
18) N. Suutala, T. Takalo and T. Moisio: Metall. Trans., Vol. 11A (1980), No. 5 717–725.
19) R.H. Espy: Welding J. (1982), No. 5, 149s–156s.